Spectroscopic studies of a fluorescent fluoresceinophane formed *via* a practical synthetic route†

Sergio Andrés Pérez Guarìn, Derek Tsang‡ and W. G. Skene*

Received (in St Louis, MO, USA) 1st August 2006, Accepted 30th November 2006
First published as an Advance Article on the web 19th December 2006
DOI: 10.1039/b611060f

A practical macrocycle synthesis incorporating a highly fluorescent fluorescein was developed. Photophysical, crystallographic and dynamic-NMR studies showed the alkyl tether forces a constrained conformation of the fluoresceinophane, which enhances the fluorescence quantum yields by reducing the excited-state deactivation pathways. Enhanced temperature-dependent fluorescence relative to its linear analogue was also found as a result of the constrained macrocycle conformation, while a manifold shift from the singlet to the triplet state still occurred in different polar solvents.

Introduction

The investigation of macrocycles has been pursued along many avenues due to their intriguing uses such as ion coordination, spectroscopic sensors, nanoactuators and molecular machines.[1–5] As interesting as their properties are, the synthesis of these compounds poses many challenges. Conventional macrocyclization approaches often require extreme dilution,[6] coordinating templates,[7–9] slow reagent addition,[10,11] ring-closing metathesis requiring expensive catalysts[12,13] and stringent reaction conditions[14] and/or and photocyclization.[15] Such approaches also suffer from extremely low yields and multiple secondary products.[16–20] These challenges have prompted many groups to develop more efficient synthetic protocols for new materials with desired functional properties.[10,11,21,22]

Our group's interest in the spectroscopic properties of fluorescein has led to the development of a practical synthetic route to macrocycles containing fluorescein. Having developed a three-step synthetic route, we have gone on to make a fluorescent macrocycle using this improved method from readily available reagents. Fluorescein was examined as the macrocycle core unit to make a fluoresceinophane because of its well characterized fluorescence properties. The resulting constrained macrocycle was expected to enhance the spectroscopic properties, including fluorescence of the fluorophore because subtle environmental changes are known to influence fluorescein's emission.[23–33] Significant fluorescent changes were anticipated for the fluoresceinophane as to make it suitable for high-temperature analyses in organic solvents. This is of particular interest because most temperature-dependent organic dyes are appropriate only for aqueous analyses. Moreover, most fluorescein derivatives are ionic in nature, which precludes their use in most organic solvents.[34,35]

This contribution reports the spectroscopic studies in addition to the crystallographic data of a fluoresceinophane that exhibits enhanced fluorescent properties relative to its linear analogue. The practical synthesis of the new fluorescent macrocycle is also presented.

Results and discussion

Synthesis of macrocycle **1** (Fig. 1) was achieved in three steps starting from fluorescein (**3**). The transformation of the neutral carboxylic acid into the methyl ester proceeds in high yield and simple precipitation affords the pure ester. This intermediate serves as the required precursor for subsequent cyclization. Alkylation of the aryl alcohol proceeds smoothly with an α-bromo-ω-alkanol with mild heating in the presence of a base. The bromoalkanol length selected at this step determines the resulting macrocycle size, which provides an attractive handle for macrocycles of different sizes.

The subsequent step, involving intramolecular cyclization for the tethered compound, was achieved by base mediated transesterification as described in Scheme 1. Interestingly, the intramolecular cyclization reaction occurred under standard reaction concentrations of 12 mM without any special dilute reaction requirements. This is in contrast to other

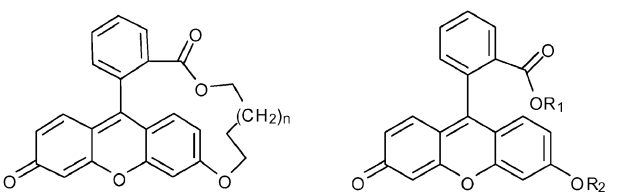

1 n = 8
2 n = 3

3 $R_1 = R_2 = H$
4 $R_1 = CH_3$; $R_2 = H$
5 $R_1 = CH_3$; $R_2 = -(CH_2)_{11}CO_2H$
6 $R_1 = CH_3$; $R_2 = -(CH_2)_{11}O(CH_2)_xCH_3$

Fig. 1 Fluoresceinophane structures and their linear analogues.

Department of Chemistry, University of Montreal, Pavillon J. A. Bombardier, C.P. 6128, succ. Centre-ville, Montreal QC, Canada H3C 3J7. E-mail: w.skene@umontreal.ca; Fax: (514) 340-5290; Tel: (514) 340-5174

† Electronic supplementary information (ESI) available: NMR spectra. See DOI: 10.1039/b611060f

‡ Current address: Department of Chemistry, University of Toronto, 80 St. George Street, Toronto ON, Canada M5S 3H6.

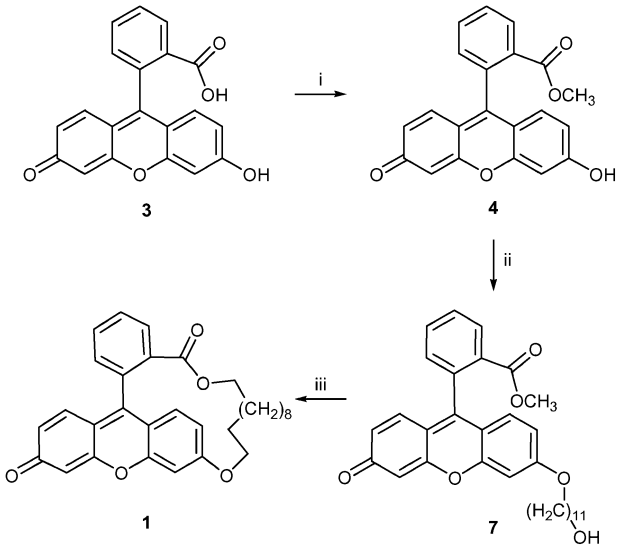

Scheme 1 *Reagents and conditions*: (i) catalytic H_2SO_4 reflux in MeOH; (ii) K_2CO_3 with $Br(CH_2)_{11}OH$ in DMF at 75 °C, N_2; (iii) NaH, DMF at 80 °C, N_2.

conventional macrocyclization approaches that often require particular reaction conditions such as extreme dilution,[6,22] coordinating templates,[7–9] slow and stepwise reagent addition,[10,11] and ring-closing metathesis.[12] Of further interest, our synthetic method does not lead to any secondary products and afforded exclusively the fluoresceinophane **1**. This is unlike many other approaches that form multiple secondary products and suffer from low yields.[16–20] The macrocycle synthesis described by this approach represents, to the best of our knowledge, one of the few examples of efficient cyclization based on a highly fluorescent core. It thus represents a viable means of forming various sized macrocycles such as **2** that incorporate the highly fluorescent fluorescein moiety.

The 1D and 2D NMR spectra of the macrocycle and its linear analogues are only subtly different. The ^1H NMR spectrum however illustrates the chiral nature of **1**. This is

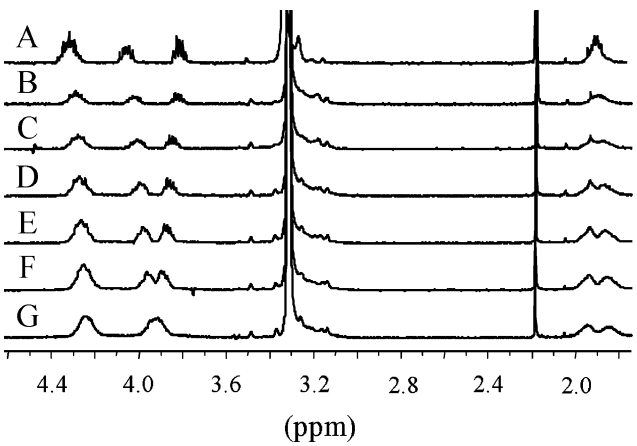

Fig. 2 Variable-temperature NMR of **1** in deuterated methanol: (A) 289, (B) 252, (C) 228, (D) 216, (E) 206, (F) 195 and (G) 185 K. Water (3.2 ppm) and MeOD (2.5 ppm) peaks are present.

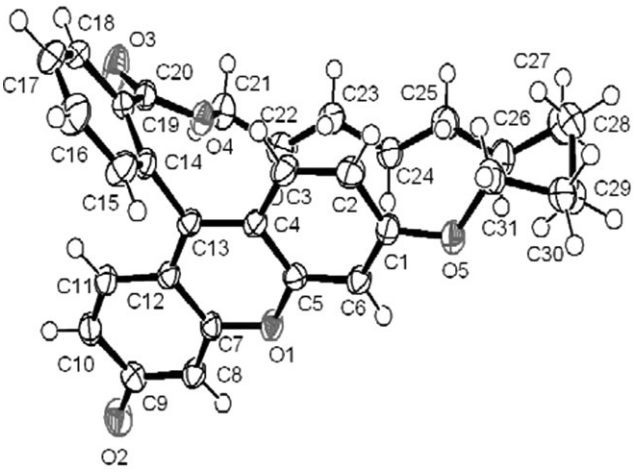

Fig. 3 ORTEP representation of crystal structure **1** with ellipsoid probability drawn at 60%.

evident from the diastereotopic methine protons observed at 3.8 ppm (Fig. 2) that are ascribed to the protons on C_{21} (Fig. 3). The NMR spectra at 500 MHz also showed the diastereotopic pattern for the protons on C_{31} at *ca.* 4.1 ppm. The presence of the chiral centers implies a significant rotational barrier around the xanthene and benzyl axis.[36,37] Coalescence of the diastereotopic methine peaks at high temperature would provide information regarding the activation energy for the rotational barrier around the xanthene–benzyl axis. Unfortunately, such high-temperature NMR measurements failed to provide any noticeable coalescence even at 425 K (see ESI†). This implies a high rotational barrier whereby the macrocycle cannot undergo complete rotation around the xanthene–benzyl axis. A lower limit of 77 kJ mol^{-1} for the free energy activation barrier around the aromatic axis can be estimated from the temperature study. A high activation barrier for rotation is supported by theoretical calculations found to be *ca.* 125 kJ mol^{-1}.[38] Similarly, low-temperature measurements provided only temperature induced chemical shifts and no coalescence. The observed variable-temperature induced shifts suggests the protons experience different environments at low temperatures, but nonetheless the macrocycle remains chiral.[39]

Confirmation of macrocycle formation for **1** and its absolute assignment was possible from its X-ray crystal structure (Fig. 3). The structure illustrates that **1** comprises two aryl units: xanthene and benzoate moieties, which are bridged by an undecanyl alkyl tether. An interesting observation is the low energetic strain induced by the tether. This is evidenced by the xanthene and benzyl moieties that adopt nearly a periplanar low-energy conformation. In fact, the tether forces the benzyl moiety to further rotate such that the mean average angle between the xanthene and benzyl planes is reduced to 73°. The 17° twist from perpendicularity allows the macrocycle to accommodate the long tether, which is clearly seen in Fig. 4. This is in contrast to known linear fluorescein derivatives that have xanthene–benzyl mean average planes that are between 85 and 90°.[40–44] The crystal structure of **1** also shows the aromatic moieties are planar, unlike other crystallographic fluorescein examples in which the xanthene is puckered.[45,46]

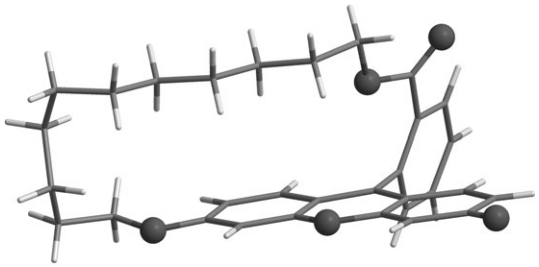

Fig. 4 Crystal structure representation of **1** showing the large volume within the fluoresceinophane. The oxygen atoms are represented as spheres for clarity.

A weak intramolecular C–H···π interaction is also present in the macrocycle, contributing to the observed conformation. This interaction occurs between C23–H15 and the centroid ring of the xanthene described by C1–C6. These are separated by 3.82 Å and H15 is rotated 151° from the mean plane of the C1–C6 aromatic centroid.

Interestingly, the flexible alkyl tether adopts a well defined rectangular conformation that is 9.7 Å wide by 3.9 Å in height. This is in contrast to an expected amorphic shape because of the high degree of freedom arising from the 11 carbon flexible aliphatic chain. π–π Stacking between the rigid xanthenes and a weak van der Waals interaction between the alkyl chains lead to the higher ordered crystal structure shown in the bottom of Fig. 5. This structure is reinforced by six CH···O weak intermolecular hydrogen bonds leading to the supramolecular network represented in the top of Fig. 5. Two such hydrogen bond interactions occur between C6–H3···O2 of two separate molecules of **1** and these are complemented by two additional bonds involving the donor–acceptor C8–H4···O1. The donor–acceptor pairs are separated by 3.344 and 3.455 Å, respectively, and form a dimer-like structure.[47] Two additional hydrogen bonds are present between two complementary molecules involving C10–H5···O3 separated by 3.348 Å.

Preliminary investigation of the ground state absorption and fluorescence was undertaken to examine the influence of the constrained cycle. In various solvents, the two spectroscopic properties observed are solvent independent (Fig. 6) with the absorption and emission centered at 456 and 560 nm, respectively. This behavior is characteristic of n–π* charge transfer transitions. Even though fluorescein is known to have many tautomers that each possess unique absorption and emissive properties,[48] the spectroscopically observed values are consistent with the quinoid structure depicted in Fig. 1. The mutual overlap of the normalized absorption and emission spectra give the absolute energy gap between the S_1 and

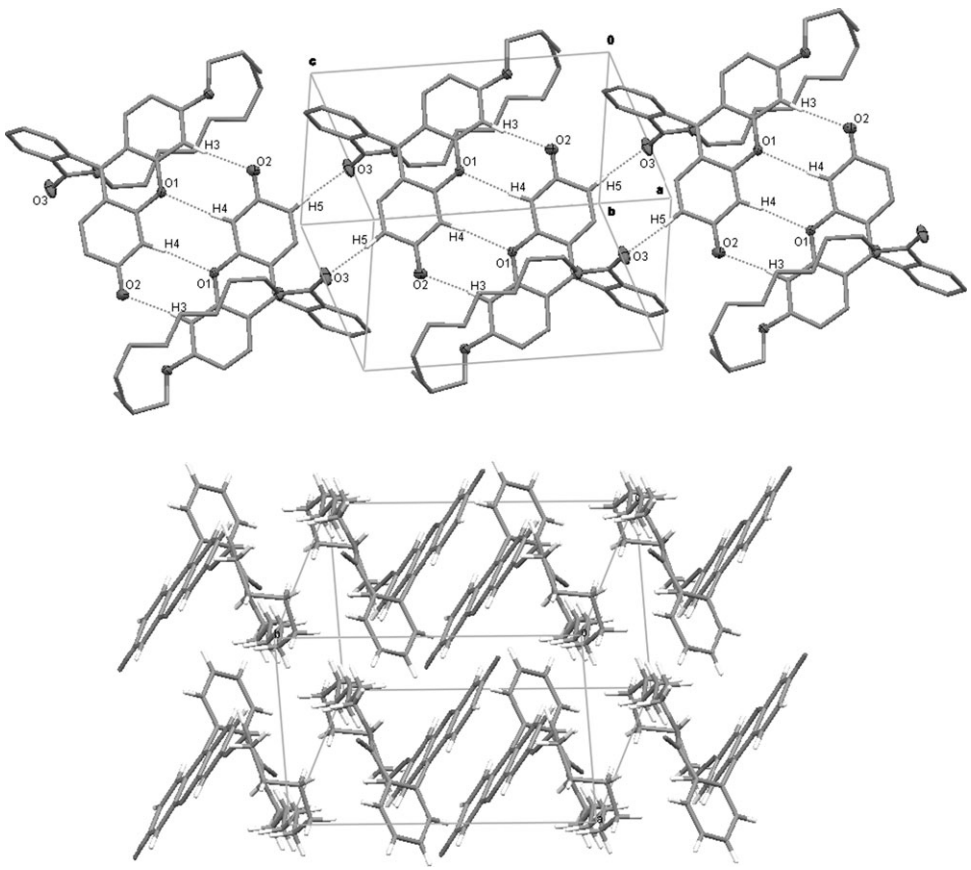

Fig. 5 Top: Schematic representation of intermolecular hydrogen bonding involving two different CH···O donor–acceptor pairs between different molecules of **1** leading to a supramolecular network. The hydrogens are omitted and the heteroatoms are drawn as ellipsoids at 50% probability for clarity. Bottom: Sheets of molecules resulting from π–π stacking between the xanthene units of different molecules and van der Waals interaction between the alkyl chains.

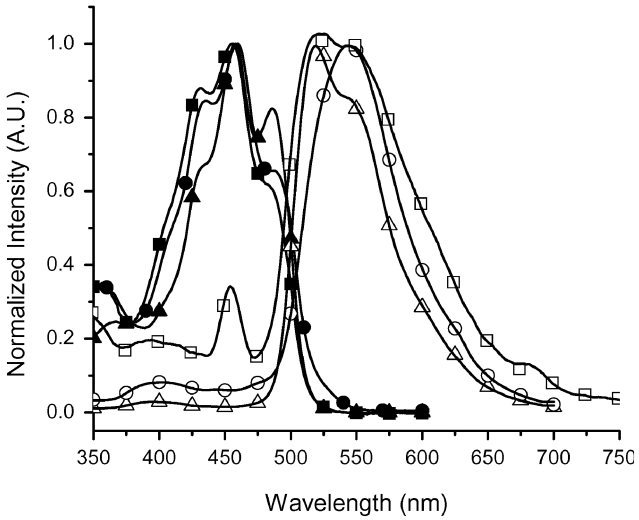

Fig. 6 Absorption spectra of **1** recorded at 25 °C in (■) acetonitrile, (▲) methanol, (●) DMSO; Fluorescence spectra of **1** in (□) acetonitrile, (△) methanol, (○) DMSO.

the S_0 states. The measured value of 239 kJ mol^{-1} is identical to previously reported values for **3**[49] and suggests that the macrocycle exerts a minimal effect on the steady-state stability of both ground and excited states at room temperature. Only a slight change in the vibrational structure was observed for the macrocycle in different polar solvents.

The tether in **1** was expected to further restrict an already hindered rotation around the xanthene–benzyl axis. It was therefore anticipated that such hindered rotation would decrease the available modes of energy dissipation and subsequently affect the fluorescent yields. As a result, enhanced fluorescence of **1** relative to **4** evidenced by an increase in quantum yield was expected. Surprisingly, the measured quantum yields for the linear and macrocycle fluoresceins reported in Table 1 are similar. Since deactivation of excited xanthene states, such as rhodamine, normally proceed by bond rotation of the substituent groups located around the xanthene core, alkylation of the phenolic group would provide an efficient means of fluorescence quenching by such a bond rotation. This is the case for **5** that exhibits roughly a 70% fluorescence reduction relative to **3**.[50] In methanol, **1** should therefore exhibit a $\Phi_{fl} \sim 0.2$. Since the measured value is three times greater than expected and is similar to **4**, the observed enhanced fluorescence implies the alkylated phenol does not undergo significant rotation. Therefore, it is not an efficient mode for fluorescence deactivation. Fluorescein on the other hand has the added pathway of rotation around the xanthene–benzyl axis for dissipating energy. The high activation barrier for rotation precludes this process as an efficient deactivation mode. The observed high fluorescence yield of **1** implies that few efficient fluorescent deactivation modes are available. The alkyl chain therefore cannot undergo efficient energy dissipation by rotation since it is linked to the benzyl moiety. This is compounded by a limited range of rotation around the xanthene–benzyl axis imposed by the tether in addition to H···H steric interaction between the two aryl groups. Such hindered rotation leads to a metronome type movement in which the two aryl groups simply swing back-and-forth in a limited range of motion of 92° compared to 120° for its linear analogue. This is further supported by the NMR results and the temperature-dependent fluorescence behavior for **1** and **4** (*vide infra*). The only mode that would significantly lead to fluorescence quenching would be a skipping rope-like motion in which the tether would rotate completely around the xanthene. This however cannot occur because the tether is insufficiently long.

The temperature-dependent fluorescence of **1** relative to its linear analogue **4** would further provide the mode of fluorescence deactivation and would demonstrate the suitability of the macrocycle as a high-temperature fluorescent probe. The temperature–fluorescence relationship in Fig. 7 shows the diminished temperature response of **1** relative to **4**. The temperature induced behavior is thoroughly reproducible without any hysteresis upon temperature cycling. In addition to calculating the fluorescence activation energies of 10 and 8.8 kJ mol^{-1} for **1** and **4**, respectively, the temperature measurements also provide information relating to the upper temperature limit for fluorescence. By extrapolating the temperature relationships, **1** is anticipated to exhibit an appreciable amount of fluorescence even at 333 °C, at which temperature the fluorescence from **4** would be completely quenched. Given that most processing of polymers occur between 200 and 350 °C,[35] the high temperature at which **1** still fluoresces makes it suitable for high-temperature fluorescence studies in organic solvents and polymer processing. This is of particular interest owing to the limited number of uncharged fluorophores. Moreover, the macrocycle could be used as an alternative highly fluorescent neutral probe for

Table 1 Fluorescent quantum yield[a] and lifetime data of fluorescein containing molecules[b] recorded at 25 °C

	1					**4**				
Solvent	Φ_{fl}	τ_{fl}/ns	Φ_T[c]	k_r[d]/10^{-8} s^{-1}	k_r[e]/10^{-8} s^{-1}	Φ_{fl}	τ_{fl}/ns	Φ_T[c]	k_r[d]/10^{-8} s^{-1}	k_r[e]/10^{-8} s^{-1}
Methanol	0.63	3.2	0.34	1.9	1.2	0.79	3.8	0.18	2.1	5.5
DMSO	0.09	1.9	0.8	0.5	4.8	0.19	1.7	0.78	1.1	4.8
Acetonitrile	0.08	1.9	0.89	0.4	4.9	0.09	0.9	0.88	1.00	1.0
Cyclohexane	0.004	2.0	0.97	0.02	4.9	—[f]	—[f]			

[a] Relative to fluorescein disodium salt ($\Phi = 0.92$) in alkaline methanol.[64] [b] $\lambda_{ex} = 456$ nm and $\lambda_{observed} = 560$ nm. [c] Calculated according to $\Phi_{IC} + \Phi_{Fl} + \Phi_T = 1$ and assuming internal conversion (IC) is 0.03.[63] [d] Calculated according to $k_r = \Phi_{fl}/\tau_{fl}$. [e] Calculated according to $k_{nr} = k_r(1 - \Phi_{fl})/\Phi_{fl}$. [f] Not sufficiently soluble for homogeneous measurements.

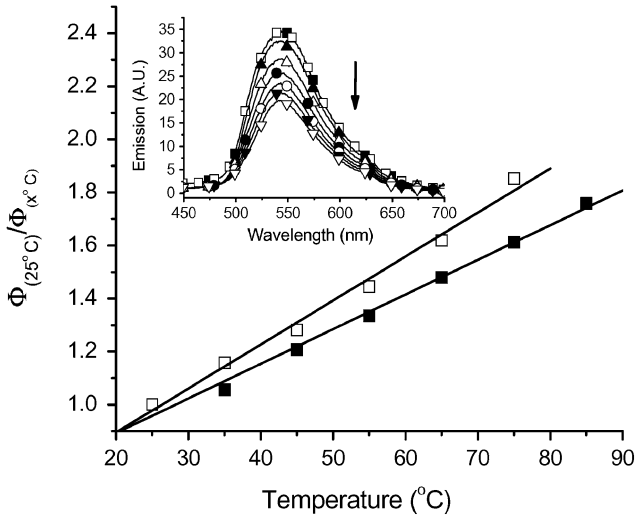

Fig. 7 Relative fluorescence change with temperature **1** (■) and **4** (□) in DMSO. Inset: Fluorescence intensity change of **1** with temperature increase in DMSO; (■) 25, (▲) 35, (△) 45, (●) 55, (○) 65, (▼) 75, (▽) 85 °C, (□) cooled again to 25 °C.

studies in organic solvents, for which there are few. Such a compound can further be used in a range of useful working temperatures without undergoing any temperature-dependent quenching, degradation, or spectral shifts,[33,34] which is not the case with most fluorescent probes.[34,35,51]

Laser flash photolysis was used to further investigate the excited-state properties of **1** and **4**. The transient absorption spectra obtained by this method, shown in Fig. 8, are similar for the linear and macrocyclic compounds. The spectra show a strong oxygen insensitive ground state bleaching component around 450 nm, which is the mirror image of the ground state absorption. The transient absorptions in acetonitrile, centered at 525 nm for **1** and 535 nm for **4**, are ascribed to the triplet

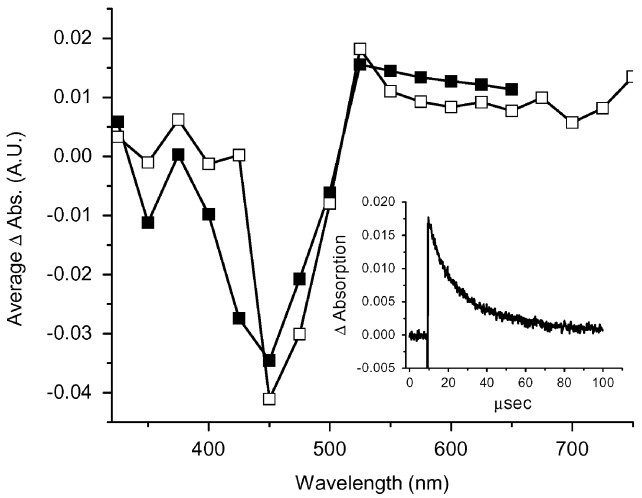

Fig. 8 Transient absorption spectra of **1** (■) and **4** (□) recorded at 19.0 and 16.8 μs, respectively, after laser excitation at 355 nm in deaerated and anhydrous acetonitrile. Inset: Triplet decay trace of **1** recorded at 525 nm in acetonitrile.

state on the basis of the observed signals that were quenched with oxygen, 1,4 cyclohexadiene and 2-methylnaphthalene, concomitant with observed monoexponential decays. Unlike other reports, the fluorescein transients exhibited only triplet formation and not any radical ionic transients.[52,53] The measured lifetimes from the monoexponential decays are 20 μs and 10 μs for **1** and **4**, respectively, that are completely quenched when the transient analyses are done in methanol. Moreover, diffusion controlled triplet state quenching with 1,3-cyclohexadiene and 2-methylnaphthalene was observed that provides an upper triplet energy limit of 173 kJ mol^{-1} for the two fluoresceins. This is approximately 25 kJ mol^{-1} lower than the corresponding fluorescein dianion triplet.[54] Unfortunately due to the strong overlapping ground state absorptions of these compounds and the typically used visible triplet probe, 2-methylnaphthalene, determination of the absolute triplet quantum yields of **1** and **4** were not possible. This is further complicated by the lack of reliable triplet molar extinction coefficients (ε) values for the neutral quinoid fluorescein triplet. A rough estimate however of $\phi_T = 0.4$ for **1** and **4** can be made through laser power dependence relative to the fluorescein dianion,[55–57] assuming the same triplet ε for the two neutral fluoresceins. The high value is further supported by the fact that no ionic transient species were observed and no nonradiative deactivation modes are known for fluorescein.[58,59]

By understanding the normal deactivation processes of fluorescent molecules, the solvent variable quantum yields observed in Table 1 can be ascribed. Typical deactivation of excited states involves quenching by solvent, increased rate of intersystem crossing leading to triplet state formation, and/or energy dissipation through bond rotation or vibrations.[60,61] The options can further be limited to two possibilities namely: nonradiative deactivation by internal conversion (IC) from $S_1 \rightarrow S_0$, and intersystem crossing from $S_1 \rightarrow T_1$.[62] Since little difference in the fluorescence monoexponential lifetimes (τ) was observed between **1** and **4** (Table 1), the same deactivation mode is expected for the two fluorescein compounds. These results combined with the steady-state fluorescence lead to the following solvent dependent observations. In polar protic solvents, the deactivation pathway is predominately from the singlet state *via* fluorescence and minor nonradiative deactivation. Conversely, intersystem crossing to the triplet state is highly favored in aprotic solvents. This manifold shift from singlet to triplet is responsible for the reduced fluorescence emission noted in Table 1, also confirmed by the observed triplet by LFP in acetonitrile. Crude estimates of the triplet formation can be calculated according to $\Phi_{fl} + \Phi_T + \Phi_{IC} \sim 1$, assuming the amount of internal conversion (IC) is minimal for the examples studied.[63] This is reasonable given the calculated nonradiative decay constants (k_{nr}) are consistent for both compounds in the various solvents. The resulting calculated triplet quantum yield is the same magnitude as those roughly obtained by laser flash photolysis. The slight polarity change appears to perturb the narrow excited singlet–triplet energies levels of the neutral quinoid fluoresceins to open an efficient means for energy dissipation *via* intersystem crossing to the triplet manifold. This is schematically represented in Fig. 9. The observed solvent behavior is similar to previous reports for fluorescein with spin orbit couplers.[48]

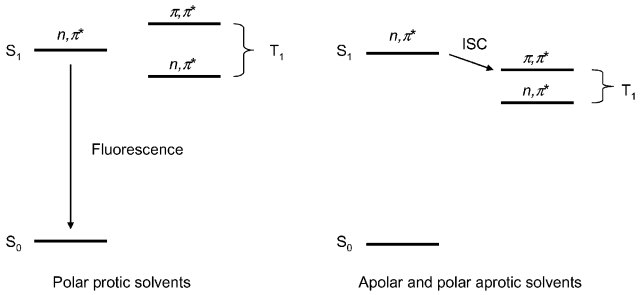

Fig. 9 Schematic representation of solvent dependent Jablonski diagram with the arrow indicating the major deactivation pathway.

Experimental

General experimental details

All reagents used were commercially obtained from Aldrich and were used without further purification except where otherwise stated. All spectrophotometric measurements were done with 10 × 10 mm cuvettes using spectroscopic grade solvents. Absorption measurements were done with a Cary 500 temperature controlled spectrophotometer and the uncorrected fluorescence measurements were performed with an Edinburgh Instruments FLS-920 combined stead-state and lifetime dual fluorimeter. The samples were deaerated with nitrogen prior to use to remove residual oxygen that would otherwise quench the excited state. The temperature was controlled with a water-circulating bath. Laser flash photolysis for triplet analyses was done with a Luzchem mini-LFP with a Continuum Sure-Lite Nd-YAG as the excitation source at 355 nm. 2D NMR spectra were recorded on a Varian 500 MHz instrument while temperature measurements were performed on a Bruker 300AX instrument.

2-(6-Hydroxy-3-oxo-3*H*-xanthen-9-yl)benzoic acid methyl ester (4). Fluorescein (**3**) (2.76 g, 8.3 mol) was dissolved in methanol (200 mL) followed by the addition of concentrated sulfuric acid (1 mL). The orange–red solution was refluxed for 12 h then poured onto ice-water (100 mL). The resulting precipitate was filtered off then chromatographed (SiO_2) with 5% methanol–dichloromethane to yield the product as an orange solid (2.76 g, 92%). Mp 228 °C. ^{1}H NMR (200 MHz, [D_4]methanol): δ 7.80 (d, 1H), 7.75 (m, 2H), 7.41 (d, 1H), 6.99 (d, 2H), 6.73 (s, 2H), 6.65 (dd, 2H), 3.59 (s, 3H). ^{13}C NMR (50 MHz, [D_4]methanol): δ 174.3, 170.0, 161.6, 160.2, 154.3, 136.6, 134.3, 133.3, 132.4, 131.6, 131.2, 13.3, 126.0, 125.6, 121.9, 117.6, 113.8, 111.6, 103.9, 103.6. FAB-MS: m/z 347.1 ([M + 1]$^+$, 100%). HR-MS(+) calc. for [$C_{21}H_{14}O_5$ + H]$^+$: 347.0914, found: 347.0920.

2-[6-(11-Hydroxyundecyloxy)-3-oxo-3*H*-xanthen-9-yl]benzoic acid methyl ester (5). To DMF (100 mL) was added 2-(6-hydroxy-3-oxo-3*H*-xanthen-9-yl)benzoic acid methyl ester (**4**) (1.67 g, 4.8 mmol) followed by potassium carbonate (1.43 g, 10.3 mmol) then 11-bromoundecan-1-ol (1.28 g, 5.0 mmol). The resulting slurry was heated to 60 °C under nitrogen for 2 days then poured onto water (300 mL). The resulting red precipitate was filtered off and washed with aqueous sodium hydroxide. The solid was subsequently chromatographed (SiO_2) with 3% methanol/dichloromethane to afford the product as a red solid (1.28 g, 52%). Mp 98–104 °C. ^{1}H NMR (200 MHz, [D]chloroform): δ 8.19 (d, 1H), 7.62 (m, 2H), 7.28 (dd, 1H), 6.86 (m, 4H), 6.46 (dd, 2H), 6.40 (d, 2-H), 4.01 (t, 2H), 3.61 (t, 2H), 3.54 (s, 3H), 1.77 (m, 2H), 1.26 (m, 20H). ^{13}C NMR (50 MHz, [D]chloroform): δ 185.7, 165.7, 163.9, 159.1, 154.4, 150.7, 134.6, 432.8, 131.2, 130.6, 129.7, 128.9, 117.4, 114.7, 114.0, 105.7, 100.8, 68.9, 62.8, 52.5, 32.9, 29.5, 28.9, 25.9, 25.9. FAB-MS: m/z 517.1 ([M + 1]$^+$, 100%).

2-(6-Hydroxy-3-oxo-3*H*-xanthen-9-yl)benzoic acid undecanoic ester (1). In anhydrous THF (40 mL) was added 2-[6-(11-hydroxyundecyloxy)-3-oxo-3*H*-xanthen-9-yl]benzoic acid methyl ester (**7**) (253 mg, 0.49 mmol) and cooled to 0 °C under argon. To this solution was added sodium hydride (380 mg, 9.5 mmol) and then the solution was allowed to warm to room temperature. The mixture was subsequently stirred for 12 h at room temperature and refluxed for 8 h under nitrogen until no starting material was detected by TLC. The solvent was eventually removed and the paste was taken up in ethyl acetate, washed with aqueous sodium carbonate and chromatographed (SiO_2) with 5% methanol–dichloromethane. The product was isolated as an orange solid (100 mg, 85%). Mp = 197–199 °C. ^{1}H NMR (200 MHz, [D]chloroform): δ 8.19 (d, 1H), 7.69 (m, 2H), 7.30 (dd, 1H), 6.93 (dd, 2H), 6.75 (s, 1H), 6.74 (d, 1H), 4.17 (t, 2H), 3.99 (m, 1H), 3.79 (m, 1H), 1.81 (t, 2H), 1.47 (t, 2H), 0.94 (m, 16H). ^{13}C NMR (50 MHz, [D]chloroform): δ 185.75, 166.15, 163.79, 158.89, 154.31, 133.67, 132.50, 131.53, 131.26, 130.42, 130.00, 129.74, 129.32, 117.66, 114.92, 112.81, 105.87, 101.53, 91.89, 67.45, 65.98, 30.96, 29.44, 28.22, 27.83, 27.66, 27.61, 27.18, 26.01, 25.07, 23.59. FAB-MS: m/z 485.4 ([M + 1]$^+$, 100%). HR-MS(+) calc. for [$C_{31}H_{32}O_5$ + H]$^+$: 485.23225, found: 485.2322.

2-(6-Hydroxy-3-oxo-3*H*-xanthen-9-yl)benzoic acid hexanoic ester (2). In DMF (70 mL) was added 2-(6-Hydroxy-3-oxo-3*H*-xanthen-9-yl)benzoic acid methyl ester (535 mg, 1.54 mmol) followed by potassium carbonate (238 mg, 1.72 mmol). The slurry was stirred for 15 min to which was then added 1,6-dibromohexane (100 µl, 0.65 mmol) and then refluxed for 3 days. The solvent was removed and the residue was taken up in ethyl acetate and then washed with aqueous sodium carbonate. The product was isolated as an orange solid (79 mg, 30%) in addition to unreacted **2** (65%) after chromatography (SiO_2) with 5% methanol–dichloromethane. ^{1}H NMR (200 MHz, [D]chloroform): δ 8.06 (d, 1H), 7.73 (m, 2H), 7.63 (m, 1H), 7.08 (d, 2H), 6.88 (s, 1H), 6.53 (d, 1H), 6.44 (s, 1H), 4.39 (m, 2H), 3.91 (m, 2H), 1.87 (m, 1H), 1.53 (m, 1H), 1.23 (4H), 0.72 (m, 2H). ^{13}C NMR (50 MHz, [D]chloroform): δ 166.9, 164.7, 132.9, 132.0, 130.0, 129.8, 116.4, 116.2, 106.5, 66.4, 29.4, 25.6, 25.09. FAB-MS: m/z 415.1 ([M + 1]$^+$, 100%).

Crystal structure determination

Diffraction data for **1** were collected on a KappaCCD diffractometer using graphite-monochromatized Mo-Kα radiation with λ = 0.710 73 Å (Table 2). The structure was solved by direct methods. All non-hydrogen atoms were refined based

Table 2 Details of crystal structure determination of **1**

Formula	$C_{31}H_{32}O_5$
M_n; $F(000)$	484.60; 516
Crystal color, form	Colorless, prism
Crystal size/mm	0.25 × 0.14 × 0.10
T/K	173
Crystal system	Triclinic
Space group	$P\bar{1}$
a/Å	7.8781(2)
b/Å	12.7652(3)
c/Å	12.8795(3)
α/°	91.972(5)
β/°	102.869(5)
γ/°	92.200(5)
V/Å^3, Z	1260.54(5); 2
D_c/g cm^{-3}	1.28
θ Range/°	2.5–30.99
Reflections: collected/independent; R_{int}	11722/8005; 0.040
μ/mm^{-1}	0.086
Abs. Corr.	None
$R1(F)$; $wR(F^2)$ [$I > 2\sigma(I)$]	0.047; 0.232
$R1(F)$; $wR(F^2)$ (all data)	0.120; 0.064
GoF (F^2)	1.083
Max. $\Delta\rho$/e Å^{-3}	0.297

on F_{obs}^2 while hydrogen atoms were refined on calculated positions with fixed isotropic U, using riding model techniques.

CCDC reference number 251400.

For crystallographic data in CIF or other electronic format see DOI: 10.1039/b611060f

Conclusion

We have demonstrated a practical three-step procedure suitable for the synthesis of macrocycles that contains a fluorescent core. The versatile synthetic method allows different tether lengths along with different fluorophores and potentially other heterocycles to be used leading to variously sized macrocycles with tunable absorption and emission properties. The practical synthetic route also allows for the easy incorporation of other steric elements that limit conformational motion of the macrocycle resulting in many interesting properties such as molecular machines. The photophysical studies showed the fluoresceinophane exhibits enhanced fluorescence owing to limited excited-state deactivation processes due to restricted motion. The macrocycle therefore is an ideal neutral fluorescence probe for high-temperature investigations in organic solvents.

Acknowledgements

The authors acknowledge financial support from the Natural Sciences and Engineering Research Council Canada, the University of Montreal, and additional equipment funding from the Canada Foundation for Innovation. D. T. thanks NSERC for a UGA scholarship. We also thank Profs. G. Cosa and D. Zargarian for helpful discussions.

References

1 V. Balzani, M. Gomez-Lopez and J. F. Stoddart, *Acc. Chem. Res.*, 1998, **31**, 405–414.
2 J. F. Stoddart and H.-R. Tseng, *Proc. Natl. Acad. Sci. USA*, 2002, **99**, 4797–4800.
3 V. Balzani, A. Credi, F. M. Raymo and J. F. Stoddart, *Angew. Chem., Int. Ed.*, 2000, **39**, 3348–3391.
4 S. J. Rowan, S. J. Cantrill, G. R. L. Cousins, J. K. M. Sanders and J. F. Stoddart, *Angew. Chem., Int. Ed.*, 2002, **41**, 898–952.
5 R. Ballardini, V. Balzani, A. Credi, M. T. Gandolfi and M. Venturi, *Acc. Chem. Res.*, 2001, **34**, 445–455.
6 J.-M. Lehn, *Supramolecular Chemistry—Concepts and Perspectives*, Wiley-VCH, Weinheim, 1995.
7 A. L. Hubbard, G. J. E. Davidson, R. H. Patel, J. A. Wisner and S. J. Loeb, *Chem. Commun.*, 2004, 138–139.
8 J. Tiburcio, G. J. E. Davidson and S. J. Loeb, *Chem. Commun.*, 2002, 1282–1283.
9 S. J. Langford and J. F. Stoddart, *Pure Appl. Chem.*, 1996, **68**, 1255–1260.
10 M. Fujita, in *Comprehensive Supramolecular Chemistry*, ed. J.-P. Sauvage, Elsevier, Oxford, 1996, vol. 9, pp. 253–282.
11 C. Dietrich-Buchecker and J.-P. Sauvage, *New J. Chem.*, 1992, **16**, 277–285.
12 C. Dietrich-Buchecker, G. Rapenne and J.-P. Sauvage, *Coord. Chem. Rev.*, 1999, **185–186**, 168–176.
13 A. D. Averin, O. A. Ulanovskaya, A. A. Borisenko, M. V. Serebryakova and I. P. Beletskayaa, *Tetrahedron Lett.*, 2006, **47**, 2691–2694.
14 A. Deiters and S. F. Martin, *Chem. Rev.*, 2004, **104**, 2199–2238.
15 K. Matohara, C. Lima, M. Yasutake, R. Nogita, T. Koga, Y. Sakamoto and T. Shinmyozu, *Tetrahedron Lett.*, 2000, **41**, 6803–6807.
16 P. Secondo and F. Fages, *Org. Lett.*, 2006, **8**, 1311–1314.
17 A. G. M. Barrett, D. Hamprecht, R. A. James, M. Ohkubo, P. A. Procopiou, M. A. Toledo, A. J. P. White and D. J. Williams, *J. Org. Chem.*, 2001, **66**, 2187–2196.
18 N. G. Lukyanenko, T. I. Kirichenko, A. Y. Lyapunov, T. Y. Bogaschenko, V. N. Pastushok, Y. A. Simonov, M. S. Fonari and M. M. Botoshansky, *Tetrahedron Lett.*, 2003, **44**, 7373–7376.
19 E. Pía, R. Toba, M. Chas, C. Peinador and J. M. Quintela, *Tetrahedron Lett.*, 2006, **47**, 1953–1956.
20 K. K. Park, H. Seoa, J.-G. Kimb and I.-H. Suh, *Tetrahedron Lett.*, 2000, **41**, 1393–1396.
21 S. Höger, *Chem. Eur. J.*, 1996, **10**, 1320–1329.
22 Y. Miyahara, *J. Org. Chem.*, 2006, **71**, 6516–6521.
23 W. H. Chan, A. W. M. Lee, Y. S. Lam and K. M. Wang, *Anal. Chim. Acta*, 1997, **351**, 197–203.
24 X. Guo, D. Zhang, Y. Zhou and D. Zhu, *J. Org. Chem.*, 2003, **68**, 5681–5687.
25 J. He, Q. Zhou and T. Shen, *Dyes Pigm.*, 1997, **34**, 219–226.
26 Z. Hong, Z. Manhua and S. Tao, *J. Photochem. Photobiol., A*, 1997, **103**, 63–67.
27 B. Jing, D. Zhang and D. Zhu, *Tetrahedron Lett.*, 2000, **41**, 8559–8563.
28 T. Konstantinova, G. Kirkova and R. Betcheva, *Dyes Pigm.*, 1998, **38**, 11–18.
29 P. Meallier, S. Guittonneau, C. Emmelin and T. Konstantinova, *Dyes Pigm.*, 1999, **40**, 95–98.
30 C. Munkholm, D. R. Parkinson and D. R. Walt, *J. Am. Chem. Soc.*, 1990, **112**, 2608–2612.
31 A. Song, J. Zhang, M. Zhang, T. Shen and J. Tang, *Colloids Surf., A*, 2000, **167**, 253–262.
32 Z.-G. Zhao, T. Shen and H.-J. Xu, *Spectrochim. Acta, Part A*, 1989, **45**, 1113–1116.
33 R. Sjöback, J. Nygren and M. Kubista, *Spectrochim. Acta, Part A*, 1995, **51**, L7–L21.
34 I. D. Figueroa, M. El Baraka, E. Quinones, O. Rosario and M. Deumie, *Anal. Chem.*, 1998, **70**, 3974–3977.
35 A. J. Bur, M. G. Vangel and S. Roth, *Appl. Spectrosc.*, 2002, **56**, 174–181.
36 A. Song, T. Wu, S. Chen, M. Zhang and T. Shen, *Dyes Pigm.*, 1998, **39**, 371–382.
37 A. Song, T. Wu, M. Zhang and T. Shen, *Chem. Lett.*, 1998, 907–908.
38 Rotation angles were determined with AM1 semi-empirical calculations.
39 A. C. Benniston, A. Harriman, P. Li, P. V. Patel and C. A. Sams, *J. Org. Chem.*, 2006, **71**, 3481–3493.

40 V. Cody, *Acta Crystallogr., Sect. C: Cryst. Struct. Commun.*, 1985, **43**, 705–707.
41 M. Tremayne, B. M. Kariuki and K. D. M. Harris, *Angew. Chem., Int. Ed. Engl.*, 1997, **36**, 770–772.
42 I. Willner, S. Marx-Tibbon, S. Cohen, Y. Eichen and M. Kaftori, *J. Phys. Org. Chem.*, 1997, **10**, 435–444.
43 K. Ajtai and T. P. Burghardt, *Biochemistry*, 1995, **34**, 15943–15952.
44 X. Wang, M. Song and Y. Long, *J. Solid State Chem.*, 2001, **156**, 325–330.
45 K. Yamaguchi, Z. Tamura and M. Maeda, *Acta Crystallogr., Sect. C: Cryst. Struct. Commun.*, 1997, **53**, 284–285.
46 I. Willner, Y. Eichen, M. R. R. Hoffman and S. Cohen, *J. Am. Chem. Soc.*, 1992, **114**, 637–644.
47 S. Dare-Doyen, D. Doizi, P. Guilbaud, F. Djedaieni-Pilard, B. Perly and P. Millie, *J. Phys. Chem. B*, 2003, **107**, 13803–13812.
48 N. I. Rtishchev, D. V. Samoilov, V. P. Martynova and A. V. El'tsov, *Russ. J. Gen. Chem.*, 2001, **71**, 1467–1478.
49 H. Zhang, Y. Zhou, M. Zhang, T. Shen, J. Xiang and J. Feng, *J. Colloid Interface Sci.*, 2003, **263**, 669–673.
50 M. Adamczyk, J. Grote and J. A. Moore, *Bioconjugate Chem.*, 1999, **10**, 544–547.
51 J. E. Whitaker, R. P. Haugland, D. Ryan, P. C. Hewitt, R. P. Haugland and F. G. Prendergast, *Anal. Biochem.*, 1992, **207**, 267–279.
52 A. I. Ponyaev, V. P. Martynova and A. V. El'tsov, *Russ. J. Gen. Chem.*, 2001, **71**, 1744–1750.
53 U. Costantino, N. Coletti, M. Nocchetti, G. G. Aloisi, F. Elisei and L. Latterini, *Langmuir*, 2000, **16**, 10351–10358.
54 S. L. Murov, I. Carmichael and G. L. Hug, *Handbook of Photochemistry*, Marcel Dekker Inc., New York, 2nd edn, 1993.
55 I. Carmichael and G. L. Hug, in *Handbook of Organic Photochemistry*, ed. J. C. Scaiano, CRC Press, Boca Raton, FL, 1989, vol. I, pp. 369–403.
56 I. Carmichael and G. L. Hug, *J. Phys. Chem. Ref. Data*, 1986, **15**, 1–250.
57 I. Carmichael, W. P. Helman and G. L. Hug, *J. Phys. Chem. Ref. Data*, 1987, **16**, 239–260.
58 B. Soep, A. Kellmann, M. Martin and L. Lindqvist, *Chem. Phys. Lett.*, 1972, **13**, 241–244.
59 D. Magde, G. E. Rojas and P. G. Seybold, *Photochem. Photobiol.*, 1999, **70**, 737–744.
60 N. J. Turro, *Modern Molecular Photochemistry*, University Science Books, Sausalito, CA, 1991.
61 T. Karstens and K. Kobs, *J. Phys. Chem.*, 1980, **84**, 1871–1872.
62 A. N. Solov'ev and V. I. Yuzhakov, *Vestn. Mosk. Univ. Ser. 3: Fiz. Astron.*, 1989, **30**, 95–97.
63 G. R. Fleming, A. W. E. Knight, J. M. Morris, R. J. S. Morrison and G. W. Robinson, *J. Am. Chem. Soc.*, 1977, **99**, 4306–4311.
64 D. Magde, R. Wong and P. G. Seybold, *Photochem. Photobiol.*, 2002, **75**, 327–334.